

AHPNW NEWSLETTER



CONTENTS

~Related News~

1. 🇰🇷 A2L refrigerants in HVAC&R industry
2. 🇯🇵 Next-generation Refrigerant Initiatives

~Research Papers~

3. 🇨🇳 Application Analyse of a Ground Source Heat Pump System in a Nearly Zero Energy Building in China



From Korea

■ A2L refrigerants in HVAC&R industry

As the industry has become more advanced, the CFC and HCFC refrigerants used in HVAC&R industry have been designated as regulated substances because of global warming and destruction of the ozone layer. As a result, HFC refrigerants, it has been used as the main refrigerant in the field of HVAC&R for more than 15 years. However, HFC refrigerants because ODP is '0', but GWP is high, causing serious problems in global warming. Recently, HFC refrigerant preventing regulations have spread worldwide, and in June 2013, the European Parliament began regulating the use of fluorine gas (F-gas) to prevent climate change. Hydrofluorocarbons (HFCs) are scheduled to be reduced by 16% compared to December 2009. The agreement of the Kigali Amendment Protocol on October 15, 2016, regulations on HFCs are being implemented worldwide. When the EU Regulation (517/2014) has been implemented from 1 January 2015, a new equipment using HFC refrigerants with a GWP of more than 2500 have been regulated until 2020. Under the Kigali Amendment, developed countries will reduce HFC emissions use first, followed by a group of Article 5 countries including China. India and nine other countries in South and West Asia will follow suit. Overall, the agreement is expected to reduce HFC use by 85 per cent by 2045. Countries are divided in three groups, as per their phase down schedules to freeze and reduce production of HFCs. The developed countries, led by the US and Europe, will reduce HFC use by 85 per cent by 2036 over a 2011-13 baseline. China, which is the largest producer of HFCs in the world, will reduce HFC use by 80 per cent by 2045 over the 2020-22 baseline. India will reduce the use of HFCs by 85 per cent over the

2024-26 baseline. The amendment also increases funding support to developing countries. The HVAC&R industry are facing to use lower GWP refrigerant. As a result, a new refrigerant with a low GWP of pure refrigerant or mixed refrigerant has been developed, which is called HFO (Hydro Fluoro Olefins). Many of these products (some existing refrigerants such as R32 and ammonia) are characterized by low flammability, and ASHRAE calls this refrigerant classification as A2L. Ammonia is classified as B2L because of toxicity. In order to expand the use of such A2L refrigerants, the International Standard Organization has recently revised the safety standards of existing refrigerating and air-conditioning equipment.

Currently, Korea does not have a clear position on the Kigali Amendment, but in reality they cannot but ratify the revised Protocol. According to the Kigali Amendment Protocol, Korea belongs to Group 1 of the A5, and will reduce HFC use by 80 per cent by 2045 over the 2020-22 baseline.

	A5 Group 1	A5 Group 2	A2
Baseline	2020-2022	2024-2026	2011-2013
Formula	Average HFC consumption	Average HFC consumption	Average HFC consumption
HCFC	65% baseline	65% baseline	15% baseline*
Freeze	2024	2028	-
1 st step	2029 – 10%	2032 – 10%	2019 – 10%
2 nd step	2035 – 30%	2037 – 20%	2024 – 40%
3 rd step	2040 – 50%	2042 – 30%	2029 – 70%
4 th step			2034 – 80%
Plateau	2045 – 80%	2047 – 85%	2036 – 85%

* For Belarus, Russian Federation, Kazakhstan, Tajikistan, Uzbekistan 25% HCFC component of baseline and different initial

The only answer is to use refrigerants that replace HFCs for these external environmental changes. The global HVAC&R industry uses A2L refrigerants or natural refrigerants, including HFO, as HFC alternative refrigerants. Europe, Japan, and the United States, which are highly regulated, already release new products using A2L refrigerants, and have revised and used safety standards to use these

Related News

refrigerants. In particular, many of the standards in the IEC 60335 series of international electrical safety standards have been recently amended to allow the use of unflammable (A2L) refrigerants to support the use of A2L refrigerants.

- IEC 60335-1:2010, Household and similar electrical appliances - Safety - Part 1: General requirements
- IEC 60335-2-24:2010/AMD2:2017, Particular requirements for refrigerating appliances, ice-cream appliances and ice-makers.
- IEC 60335-2-40:2018, Particular requirements for electrical heat pumps, air-conditioners and dehumidifiers
- IEC 60335-2-89:2010/AMD2:2015, Particular requirements for commercial refrigerating appliances with an incorporated or remote refrigerant unit or compressor

These standards provide the conditions of use of the A2L refrigerant to ensure maximum safety during the application of this refrigerant. The main difference between A1 refrigerants such as R-410A, R-134a and R-407C and A2L refrigerants such as R-32, HFO R-1234yf and HFO R-1234ze is the velocity to propagate flames. A2L refrigerant is burned but burning speed is less than 10cm/s, which is lower than the burning rate of A3 refrigerant such as R-290 which actually explodes when ignited. Actually, it is very difficult for A2L gas to ignite, but precautions must be taken to prevent accidental accumulation of refrigerant during system charging. The manufacturer proposes to use an extraction fan, especially when the outdoor unit is in an enclosed space. International and European safety standards, such as ISO 5149 and EN 378, provide a requirement to keep flammability limits far below accidental leaks.

As of January 1, 2017, all new cars produced in Europe should only use refrigerants with a GWP of less than 150 in

the air conditioning system. The current available refrigerant is HFO R-1234yf. The automotive industry has conducted thorough testing and risk assessment before using R-1234yf to confirm that it is a refrigerant to replace R-134a. R-32 (HFC classed as A2L) is now widely sold as an alternative to R-410A in new air conditioning and heat pump systems because of its performance similarity to R-410A. Regulations for the use of A2L refrigerants differ from those in Europe, but in Japan many room air conditioners already used R-32 refrigerants. Some large chillers use R-1234ze instead of R-134a, while R-1234ze is an HFO and is classified as A2L but is actually a nonflammable refrigerant at temperatures below 300°C. Because R-1234yf is closer to the performance of R-134a, the system is suitable for use in refrigeration system designed to use low flammable refrigerants. Because there is no flammability at room temperature, R-1234ze is also used for some aerosol applications. Currently, refrigerant manufacturers are developing A2L HFO blends with alternative refrigerants such as R-404A and R-410A.

Internationally, the use of low GWP refrigerants according to the HFCs refrigerant withdrawal scenario to prevent global warming is a global trend. Accordingly, the international standards for the safety standard of the heat pump, the air conditioner and the dehumidifier have been revised to use the A2L refrigerant. However, Korean safety standards still use the old version which cannot use this refrigerant. Already, many countries such as Europe, USA, and Japan have been introducing products using A2L refrigerant to the market and gradually expanding the market. Recently Korea National TC(Technical Committee) are working to urgently revise the existing safety standards so that A2L refrigerant can be used in Korea by reviewing current international standards. The revised versions will be available the middle of 2019. Afterwards, it is necessary to hasten to advance into

overseas market by expanding the domestic market of A2L refrigerant products and improving this technology by matching domestic KC (Korea Certificate) standards with the latest version of IEC.

● From Japan

■ Next-generation Refrigerant Initiatives

–Report on Kobe Symposium 2018

The International Symposium on New Refrigerants and Environmental Technology 2018 (Kobe Symposium) was held at the Kobe International Conference Center and organized by the Japan Refrigeration and Air Conditioning Industry Association (JRAIA). The 13th edition of the symposium started on December 6 and ended with success on December 7.

Around 550 people from Japan and around the world participated in the symposium, a conference size second only to the 2016 symposium. Many timely topics were covered with content significant to the industry, indicating the high level of interest worldwide in environmental and refrigerant initiatives.

Many of the presentations at the symposium focused on global warming countermeasures, with topics including new heating, ventilation, air conditioning, and refrigeration (HVAC&R) equipment and new refrigerant technology development contributing to environmental conservation as well as the latest regulatory developments in Japan and abroad.



Tetsuji Okada, president of JRAIA presents his keynote speech at Kobe Symposium

The Kigali Amendment, which was adopted at the 28th Meeting of the Parties to the Montreal Protocol (MOP28) in October 2016 in Kigali, Rwanda, came into force in January 2019, and countries are now working to meet their commitments under it. The Kigali Amendment to the Montreal Protocol was ratified by 60 parties as of November 12, 2018, which triggered its entry into force. While the obligations of the respective parties to implement environmental initiatives and the speed of their implementation vary along with their different political and economic circumstances, all parties recognize the urgency with which action on climate change needs to be taken.

The symposium began with opening remarks by Toshiyuki Takagi, chairman of the board, JRAIA, and Masatoshi Omura, executive director, Kobe Tourism Bureau. Over the two days of the meeting, participants had the opportunity to attend a wide range of technical sessions, poster sessions, and presentations.

Related News



Xudong Wang, AHRI, reports on research on flammable refrigerants

The session started with a keynote address by Tetsuji Okada, president of JRAIA, titled ‘History of the Kobe Symposium and the Latest Issues of the HVAC Industry,’ which covered the history of the symposium, market trends, the latest developments in regulations and protocols, and global environmental protection policy and efforts.

Technical Session 1 focused on environmental issues. Toshio Kosuge from Ministry of Economy, Trade and Industry (METI) discussed the amendment to Japan’s ozone layer protection law. Presentations on the F-gas Regulation, the hydrofluorocarbon (HFC) phasedown, Ecodesign legislation, and safety standards in Europe were made by Mihai Scumpieru and Els Baert from the European Partnership for Energy and the Environment (EPEE). Xudong Wang from the Air-Conditioning, Heating, and Refrigeration Institute (AHRI) reported its research on flammable refrigerants.

A presentation titled ‘Updates on Standards Development and Revision in the Chinese R&AC Industry Following the Kigali Amendment’ was made by Huicheng Liu from the China Refrigeration and Air Conditioning Industry Association

(CRAA).

Appliance manufacturers talked about new refrigerants during technical sessions 2 and 3, and lectures on the safety of refrigerants and risk assessments were delivered during technical sessions 4 and 5. Technical Sessions 6 and 7 covered compressors and lubricants. Speakers delivered presentations on energy conservation in Technical Session 8. Finally, during Technical Session 9, refrigerant manufacturers presented their findings on new refrigerants.



Around 550 people from Japan and around the world participated in the symposium

The sessions at the symposium gave updates on topics covered at the Kobe Symposium 2016 and on progress in refrigerant development and HVAC&R technology, among others. A2L refrigerant assessments were the main topic discussed at the Kobe Symposium 2016. For the 2018 edition, in addition to A2L refrigerants, propane (R290) and other A3-class refrigerants were discussed for the first time. Many presenters reported on the results of their verification experiments with these refrigerants. There were also many reports on alternative refrigerants to R410A and R404A. Other presentations discussed equipment development and experimental findings for new low-global warming potential (GWP) refrigerants that achieve high efficiency such as R466A, R463A, and R448A. Issues of stability and safety, namely flammability,

Related News

for new refrigerants are not yet settled topics, and these refrigerants may ultimately not prove to be the solutions the industry is looking for. However, these new refrigerants and the HVAC&R technical developments related to them do shine a light on global-scale environmental initiatives and have the potential to lead to future developments.

JARN had opportunities to interview many lecturers individually during the symposium. They include Stephen Kujak from Trane, who gave a presentation titled, 'Update on Next Generation Low GWP Refrigerants for Chiller Products,' Masato Fukushima from AGC, who talked about 'Next Generation Low-GWP Refrigerants AMOLEA,' and Dr. Sarah Kim from Arkema, who delivered a lecture titled, 'Flammability and Risk Assessment of Low Environmental Impact Refrigerants for R134a and R404A Replacement.' JARN plans to publish these interviews in future issues.

of the Kobe Symposium a venue for disseminating information on new technologies related to refrigerants and compressors. ”

The Kobe Symposium brings together HVAC&R experts not only from Japan but also from around the world to share the latest information on refrigerant issues that are some of the most important topics in the industry today and as such, is set to attract even more attention in the coming years.

(source : 2019/1/25,JARN)



The Kobe International Conference Center In an interview with JARN, Tetsuji Okada, president of JRAIA, commented, “ This year ’ s Kobe Symposium recorded the second-highest attendance ever. Experts from around the world praised the impressive content offered at this symposium. I intend to make future editions

A new performance index for air-source heat pumps based on the nominal output heating capacity and a related modeling study

Wei Wang, Yiming Cui, Yuying Sun, Xu Wu, Shiming Deng
Beijing University of Technology, Hong Kong Polytechnic University, China

Abstract

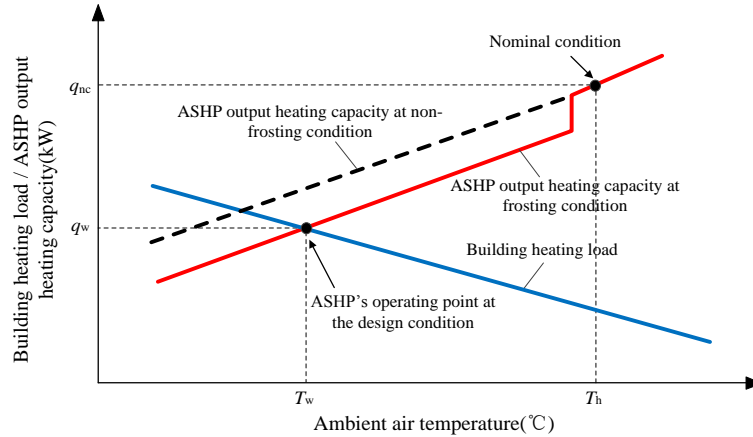
Air source heat pump (ASHP) units have been widely used for space heating in recent years. While a space heating ASHP unit is normally rated at its nominal operating condition. However, during its actual space heating operation, it rarely works at the nominal condition. The actual output heating capacity can remarkably deviate from that at the nominal condition, due to the influences of ambient air temperature and frosting-defrosting operation. Therefore, to enable a comprehensive and convenient evaluation of the operating performance of ASHPs with frosting-defrosting operation and to provide designers with appropriate design guidelines to size a space heating ASHP unit, a new performance index has been proposed. The new performance index, ε_{NL} , or the loss coefficient in the nominal output heating energy, was actually based on the nominal output heating capacity of ASHP units, which was readily available and stayed unchanged irrespective when and where ASHPs were operated. In this paper, the defining of ε_{NL} was firstly given following a detailed explanation of the frosting-defrosting operation of an ASHP unit. Secondly, a GRNN model for predicting the ε_{NL} of a field ASHP unit was established following a correlation analysis using a total of 473 groups of field measured data from a field ASHP unit. Finally, a modeling study using the developed GRNN model was carried out, and the study results suggested that defrosting initiating time would affect the ε_{NL} , and there may exist an optimal defrosting initiating time at which ε_{NL} was at its minimum, and that an increase in ambient air relative humidity or a decrease in ambient air temperature would result in an increase in ε_{NL} .

1 Introduction

Due to the advantages of high efficiency and environmental protection, air-source heat pump (ASHP) units have been widely accepted all over the world [1]. Europe Union, Japan and China successively identified the ASHP technology as one of the renewable energy utilization technologies. The Department of Energy (DOE) in the US also regarded it as one of the most potential air conditioning technologies in the 21st century. Since the 1990s, ASHP units have been widely used for both space cooling and heating in cold, hot-summer and cold-winter regions in China [2-3]. Recently, coal-electricity conversion projects in an attempt to alleviate severe air pollution in northern China as a result of using coal for space heating further increased the scale of the applications of ASHP technology [4]. In 2017, 2.9 million number of ASHP units were sold in China, representing an increase of 43.7% from that in 2016. It is expected that the Chinese ASHP market will continue to grow at a yearly increasing rate of more than 20% over the next five years [5].

A space heating ASHP unit is usually rated at its nominal operating condition in terms of operating efficiency and output heating capacity. However, during its actual space heating operation, it rarely works at the nominal condition [6-7]. Ambient air temperature and frosting-defrosting can significantly affect the actual operating performance of ASHP units [6, 8-10]. Fig. 1 shows the variation of the output heating capacity of an ASHP unit during actual space heating operation [11-12]. At a non-frosting condition, the actual output heating capacity decreases as ambient temperature decreases and is usually lower than its nominal heating capacity. At a frosting condition, the actual output heating capacity further decreases compared to that at the non-frosting condition, as a result of frosting-defrosting effect. It can be seen from Fig.1 that at the frosting condition, the actual output heating capacity of the ASHP unit can remarkably deviate from that at the nominal condition. Furthermore, different

frosting conditions, e.g., severe, moderate and mild, can also affect the actual output heating capacity of an ASHP unit [13].



q_{nc}	Nominal output heating capacity	q_w	Building heating load at the design
T_h	Outdoor air temperature at the nominal condition ($^{\circ}\text{C}$)	T_w	Outdoor air design temperature for winter space heating ($^{\circ}\text{C}$)

Fig. 1 Variations in the actual output heating capacity of a space heating ASHP unit/building heating load with the changes in actual operating ambient air temperature

Various approaches have been used to evaluate the operating performances of ASHP units during frosting and defrosting operations. Lu [14] and Shi et al. [15] used a heating season performance factor, which reflected the operating efficiency of ASHP units during an entire heating season. Ameen [16] and Jiang et al [17] evaluated the operating performances of ASHP units during frosting and defrosting by using a loss coefficient of frosting-defrosting, which was defined as the ratio of the COP during a frosting operation to that during a non-frosting operation at the same ambient air temperature. Zhu et al. [18] proposed to use an index of heating efficiency to evaluate the operating performance of ASHP units during frosting and defrosting, which was the ratio of the output heating capacity during a frosting operation to that during a non-frosting operation at the same ambient air temperature. To evaluate ASHPs' operating performances, Li et al. [19] developed a generalized performance model for an ASHP unit in a single frosting-defrosting cycle and proposed to use system COP, which was the ratio of the total output heating capacity to the total power input during the complete frosting-defrosting cycle, to evaluate its operating performance.

As seen, although there have been extensive research efforts in developing suitable indicators for evaluating the operating performances of ASHP units, there were a number of inadequacies in assessing the operating performances of ASHP units during a complete frosting and defrosting cycle when using these indicators. Firstly, certain evaluation methods [14-15,19] only looked at the actual operating efficiency of an ASHP, without considering the loss in operating performances due to frosting and defrosting. Secondly, other methods [16-17] only took the frosting operation in a frosting-defrosting cycle into account, without considering the defrosting operation. Thirdly, although a number of evaluation indexes considered the ratio of heating capacity/COP during the frosting operation to those during the corresponding non-frosting operation at the same ambient air temperature [16-18], the actual output heating capacity or COP during the corresponding non-frosting operation were variable and thus difficult to obtain, so that these evaluation indexes were hardly applied to practice. On the other hand, in most previous studies, only the frosting-defrosting performances of ASHP units at certain typical operating conditions were assessed by field tests. The performances at all frosting-defrosting operating conditions were however difficult

to be evaluated using field tests due to high project cost and long project duration involved. Furthermore, no previously developed performance indicators were based on the performance loss against that at nominal conditions, leading to potential system oversizing, as the sizing of ASHPs was usually based on the performance data at the nominal condition provided by ASHPs' manufacturers.

Therefore, to comprehensively and conveniently evaluate the frosting-defrosting performances of ASHPs and to provide ASHP systems designers with an appropriate design guideline regarding the actual operating performances during frosting and defrosting, a loss coefficient in nominal output heating energy as a new frosting-defrosting performance evaluation index for space heating ASHP units has been proposed. In this paper, firstly, a detailed account of the frosting-defrosting operation of an ASHP and the definition of the proposed loss coefficient are given. Secondly, the development of a Generalized Regression Neural Network (GRNN) based mathematical model for predicting the proposed loss coefficient is reported. Thirdly, a modeling study using the developed GRNN based model is presented. Finally, a conclusion is given.

2 The operating performances of an ASHP unit during frosting-defrosting operation

Fig. 2 conceptually shows the frosting-defrosting operation, with only 2 cycles, of a space heating ASHP unit. As seen, a complete frosting-defrosting cycle is made of a frosting operation and a defrosting operation, and there can be a number of frosting-defrosting cycles in a heating operation of several hours. The operating performances of an ASHP in terms of its output heating capacity during a frosting-defrosting cycle are influenced by:

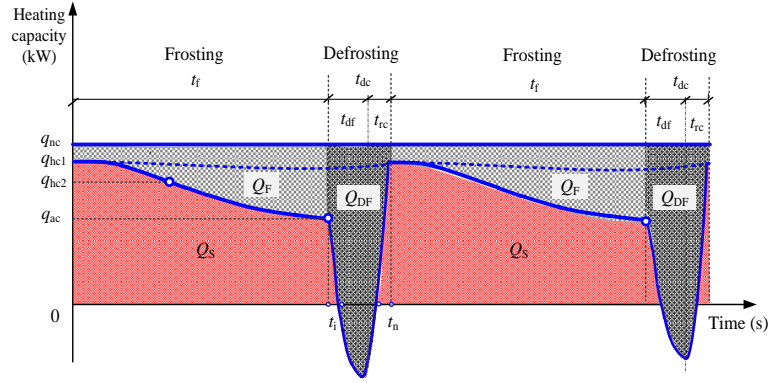
1) Ambient air temperature

As shown in Fig. 2, at a non-frosting operation, when actual operating ambient air temperature is lower than the ambient air temperature at the nominal condition, the actual output heating capacity (q_{hc1}) is lower than nominal heating capacity (q_{nc}). The difference between q_{hc1} and q_{nc} is due to the difference between ambient air temperature at the nominal condition and the actual operating ambient air temperature.

2) Frosting-defrosting operation

As also shown in Fig. 2, a complete frosting-defrosting cycle for an ASHP unit includes a frosting operation and a defrosting operation. In the frosting operation having a duration of t_f , as the operation proceeds, the actual output heating capacity from the ASHP unit continues to decrease as frost continuously deposits on its outdoor coil surface. At t_i , the ASHP unit starts defrosting and enters the defrosting operation having a duration of t_{dc} . The entire defrosting operation may be further divided into a defrosting period and a heating restoration period, as shown in Fig. 2. When the actual output heating capacity returns to q_{hc1} , the defrosting operation ends and a new frosting-defrosting cycle starts.

Furthermore, the loss in the nominal heating capacity is closely related to when defrosting starts. If defrosting starts earlier, the reduction in nominal heating capacity will be lower, but with a shorter frosting operation. However, earlier defrosting leads to more frosting-defrosting cycles in a heating operation of a fixed time duration. On the contrary, if defrosting starts later, the loss in nominal heating capacity during frosting operation will be greater, with a longer frosting operation and fewer frosting-defrosting cycles.



t_i	Defrosting starting time (s)	t_n	Defrosting ending time (s)
t_f	Frosting operation duration/defrosting initiating time (s)	t_{df}	Defrosting period (s)
t_{rc}	Heating restoration period (s)	t_{dc}	Defrosting operation duration (s)
q_{nc}	Nominal output heating capacity (kW)	q_{hc1}	Instantaneous output heating capacity at normal operating condition (kW)
q_{hc2}	Instantaneous output heating capacity at frosting condition (kW)	q_{ac}	Instantaneous output heating capacity before defrosting operation (kW)
Q_F	Nominal frosting energy loss (kJ)	Q_{DF}	Nominal defrosting energy loss (kJ)
Q_S	Effective heating energy (kJ)		

Fig. 2 Frosting-defrosting operations of a space heating ASHP unit

Based on the above analysis and Fig. 2, a loss coefficient in the nominal output heating energy, ε_{NL} , was proposed, as follows:

As shown in Fig. 2, a nominal frosting energy loss, Q_F , was defined as the loss in the nominal heating energy during the frosting operation in a complete frosting-defrosting cycle, as follows:

$$Q_F = \int_0^{t_f} (q_{nc} - q) dt_c \quad (1)$$

The loss coefficient in the nominal heating energy during the frosting operation, ε_F , was defined as the ratio of the nominal frosting energy loss to the total available nominal output heating energy during a complete frosting-defrosting cycle, as follows:

$$\varepsilon_F = \frac{Q_F}{\int_0^{t_n} q_{nc} dt} \quad (2)$$

A nominal defrosting energy loss, Q_{DF} , was defined as the loss in the nominal heating energy during the defrosting operation in a frosting-defrosting cycle, as follows:

$$Q_{DF} = \int_{t_i}^{t_n} (q_{nc} - q_{hc2}) dt \quad (3)$$

The loss coefficient in the nominal heating energy during defrosting operation, ε_{DF} , was defined as the ratio of the nominal defrosting energy loss to the total available nominal heating energy during a complete frosting-defrosting cycle, as follows:

$$\varepsilon_{DF} = \frac{Q_{DF}}{\int_0^{t_n} q_{nc} dt} \quad (4)$$

Then, the loss coefficient in the nominal heating energy, ε_{NL} , in a complete frosting-defrosting cycle was defined as the sum of the loss coefficient in the nominal heating energy during the frosting operation, ε_F , and that during the defrosting operation, ε_{DF} , as follows:

$$\varepsilon_{NL} = \varepsilon_F + \varepsilon_{DF} \quad (5)$$

ε_{NL} was defined based on the nominal output heating capacity of an ASHP unit during a complete frosting-defrosting cycle, and can, therefore, be used to comprehensively reflect the

loss in the nominal heating energy during a complete frosting-defrosting cycle. Since the nominal heating capacity of an ASHP unit is readily available from its manufacturer, and would not vary irrespective where and when the ASHP unit is operated, therefore, the operating performances of the ASHP unit during a complete frosting-defrosting cycle can be evaluated comprehensively and conveniently.

3 Development of a GRNN model for predicting ε_{NL}

With the above defined ε_{NL} for an ASHP unit, a comprehensive and convenient index to evaluate the operating performances of ASHP units with frosting-defrosting operation was proposed. However, to comprehensively and conveniently evaluate the operating performances of an ASHP unit in practice, it was necessary to obtain values of ε_{NL} under all different ambient and operating conditions. Experimental/field studies can be employed to evaluate ε_{NL} for an ASHP unit, but it was difficult to get its performances at all frosting-defrosting operating conditions due to high project costs and long project duration involved. Therefore, mathematical modeling approach for evaluating and predicting ε_{NL} values based on limited number of experimental or field testing data was preferred. While there existed a large number of modeling approaches, artificial neural network modeling has been one of the most powerful and popular tools for establishing mathematical models. Therefore, as one of artificial neural network modeling methods, Generalized Regression Neural Network (GRNN) was adopted to evaluate and predict ε_{NL} values at different frosting-defrosting conditions due to its advantages of faster training speed [20] and simple network architecture [21-22]. When developing the GRNN based model for evaluating and forecasting ε_{NL} in the study reported in this paper, firstly, field tests were carried out from 2012 to 2016 heating seasons using a field ASHP unit installed in Beijing, China, and 473 groups of field measured performance data obtained. Then, through a correlation analysis, the main factors affecting the ε_{NL} of the field ASHP unit were determined and used as the input parameters to the GRNN model for predicting the ε_{NL} for field ASHP unit to be developed. Thirdly, the GRNN model for predicting ε_{NL} with the determined input parameters was trained and tested using the 473 groups of field measured data. Finally, a modeling study using the developed GRNN model on the impacts of varying ambient parameters and defrosting initiating time on ε_{NL} was carried out.

3.1 Field test

3.1.1 Test setup

The field tests were conducted with a field ASHP unit serving an office building in Beijing, China. There were 11 rooms in the office building with a total heating floor area of 185 m². Fig. 3 shows the schematics of the field test setup. As seen, the test setup consisted of the field ASHP unit and a space heating system for the building. The field ASHP unit with a constant speed compressor was employed as the heating source for the building. The nominal heating capacity of the ASHP unit and power input to the ASHP unit were 14 kW and 4.3 kW, respectively. On the other hand, the space heating system was made of fan coil units and hot water circulating pumps, etc.

During 2012 to 2016 heating seasons when the field tests were carried out, various defrosting initiating methods, such as Temperature-Time (T-T), Tube-Encircled Photoelectric Sensors (TEPS) [23] and Temperature-Humidity-Time (T-H-T) [24], for the field ASHP unit were applied, leading to its varied frosting operation durations. In addition, a measuring system was installed to measure and record the testing ambient environmental conditions and the operating parameters of the field ASHP unit. Table 1 shows the detailed information of the measuring system, for the following parameters:

- Air side: ambient air temperature and relative humidity, outdoor coil air outlet temperature and relative humidity, air side pressure drop across the outdoor coil;
- Refrigerant side: temperature of the outdoor coil surface, temperatures and pressures at the suction and discharge of compressor;
- Water side: hot water temperatures at the inlet and outlet of the indoor coil in the field ASHP unit, hot water mass flow rate;
- Others: power inputs to the compressor, hot water pump and fan in the field ASHP unit, mass of melted frost, etc.

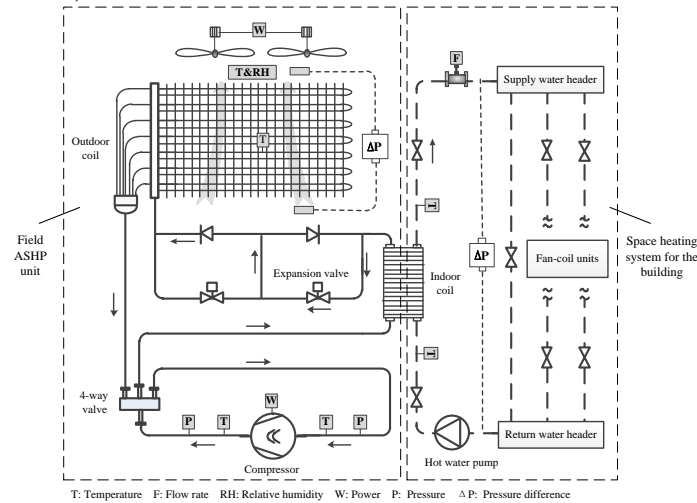


Fig. 3 Schematics of the field test setup

Table 1 Details of the measuring /sensors devices

Sensors/devices	Number	Accuracy	Full scale
Temperature sensor (PT1000)	14	± 0.15 °C	-40~140 °C
Temperature, humidity sensor	2	± 0.15 °C; ± 5 %	-20~70 °C; 0~100 %
Pressure sensor	4	± 0.4 %	0~40 bar; 0~25 bar
Power meter	1	± 1.0 %	--
Flow meter	1	± 0.5 %	$0.5 \sim 10 \text{ m}^3 \text{ h}^{-1}$
Digital camera	1	--	14 Megapixels
Electronic scale	1	± 0.1 g	0~6000 g

3.1.2 Test cases and conditions

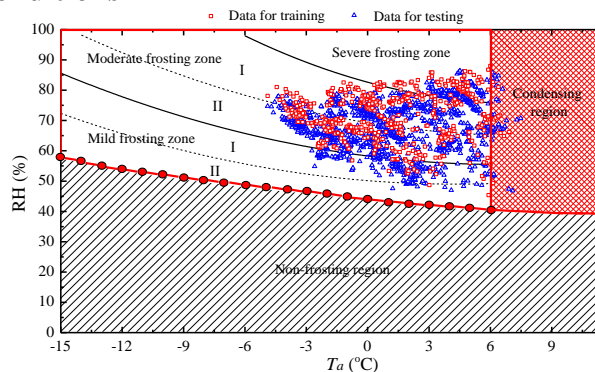


Fig. 4 Ambient air states of the 473 groups of field measured data plotted on the frosting map [13]

The field studies using the field ASHP unit from 2012 to 2016 heating seasons resulted in a total of 473 groups of field measured data. The ambient air temperature and relative humidity at which the 473 groups of data were obtained are illustrated on a frosting map [13] shown in Fig. 4. As seen, the ambient air temperature ranged from -4°C to 7°C and the relative humidity from 45% to 85%, located in the severe, moderate and mild frosting zones of the frosting map. In addition, with various defrosting initiating methods applied, varied frosting durations of 10 to 85 minutes were resulted in.

The 473 groups of field measured data contained the following ambient and operating parameters for the field ASHP unit, with their ranges and averages shown in Table 2.

Table 2 Details of the 473 groups of field measured data

Parameters		Range	Average	unit
Ambient air temperature	T_a	-4~7	1.5	$^{\circ}\text{C}$
Relative humidity	RH	45~85	68.7	%
Defrosting initiating time	t_f	10~85	34	min
Nominal frosting energy loss	Q_F	0.15~15	3.6	kJ
Defrosting period	t_{df}	150~300	226	s
Nominal defrosting energy loss	Q_{DF}	3~6	4.2	kJ
Instantaneous output heating capacity before defrosting	q_{ac}	6.0~13.2	8.9	kW
Mass of melted frost	$M_{f,m}$	0.1~2.8	0.79	kg
Water supply temperature	T_{ws}	38.6~41.1	39.8	$^{\circ}\text{C}$
Water return temperature	T_{wr}	36.2~38.9	37.6	$^{\circ}\text{C}$
Loss coefficient in the nominal	ε_{NL}	13.0~48.1	33.4	%

3.2 Input parameters of the GRNN model

In order to determine the ambient and operating parameters affecting ε_{NL} of the field ASHP unit, an analysis on the correlation between ε_{NL} and all the other parameters listed in Table 2 except Q_F and Q_{DF} based on the Pearson correlation coefficient (r) method [25] using the 473 groups of field measured data was conducted, and the analysis results are given in Table 3. The reasons that Q_F and Q_{DF} were not included in the analysis were because they were related to ε_{NL} .

Table 3 Correlation test results of the field measured data

Parameters		Pearson correlation coefficient (r)
Ambient air temperature	T_a	-0.45
Relative humidity	RH	0.35
Defrosting initiating time	t_f	-0.12
Defrosting period	t_{df}	0.59
Instantaneous output heating capacity before defrosting	q_{ac}	-0.54
Mass of melted frost	$M_{f,m}$	-0.143
Water supply temperature	T_{ws}	0.07
Water return temperature	T_{wr}	0.06

The results shown in table 3 suggested that all these parameters were correlated with ε_{NL} , but with varying degree of correlation. However, t_{df} , q_{ac} and $M_{f,m}$ may be considered as dependent parameters as they were also affected by T_a , RH and t_f , and therefore, they were not used as the input parameters to the GRNN model. Furthermore, during the field tests, the variations in T_{ws} and T_{wr} were relatively small at less than 7.5%, as compared to those of other parameters. Therefore, the influences of water temperatures on ε_{NL} were small and the two parameters were not used either as the input parameters to the GRNN model.

Consequently, as shown in Equation (6), following the above analysis, T_a , RH and t_f were used as the input parameters to the GRNN model to be developed.

$$\varepsilon_{NL} = f(T_a, RH, t_f) \quad (6)$$

3.3 Training and testing of the GRNN model

The totally available 473 groups of field measured data were used for training and testing the GRNN model. Since there were no specific guidelines available on allocating the percentage of the total data groups for either training or testing [26], and with reference to previous studies using 75% [27] or 80% [28] of data groups for training, therefore, when developing the GRNN model, a total of 362 data groups, or 76.5% of the total data groups, were used for training the GRNN model and the remaining 111 data groups, or 23.5%, for testing the GRNN model. Furthermore, when allocating the data groups for training and testing, the distributions of the ambient parameters on the frosting map [13] for both groups were similar.

3.3.1 Training of the GRNN model

As mentioned, when developing the GRNN model, T_a , RH and t_f were assigned as the input parameters to the GRNN model, and ε_{NL} as the output parameter. Fig. 5 shows the structure of the GRNN model for predicting ε_{NL} .

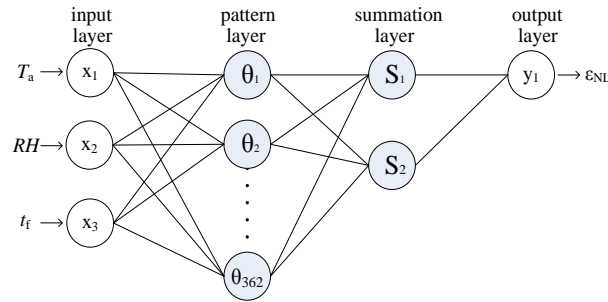


Fig. 5 The structure of the GRNN model for predicting ε_{NL}

As seen there were four layers in the GRNN model, an input layer, a pattern layer, a summation layer and an output layer. The input layer was made of three simple distributed neurons, which can directly pass the three input parameters, i.e., T_a , RH and t_f , to the pattern layer, where there were 362 neurons representing the 362 groups of data for training. The Gaussian function was used as the transfer function. In the summation layer, there were two different kinds of neurons, one to sum the outputs from all the neurons in the pattern layer and the other the weighted the outputs from all the neurons in the pattern layer. Finally, the output layer consisted of only one neuron representing ε_{NL} .

Once data groups for training were determined, the weights for each neuron in the network structure were also determined. A smooth factor, σ , which can be used to indicate the performances of the GRNN model for predicting ε_{NL} , needed to be determined by using the Cross Verification method [20, 29], based on the expected error percentage, EEP [20], shown in Equation (7).

$$EEP = \sqrt{\frac{\sum_{i=1}^{362} (\hat{y}_i - y_i)^2}{362}} \times 100\% \quad (7)$$

Where, \hat{y}_i and y_i are i^{th} predicted and measured ε_{NL} values out of the total 362 data groups, and y_{\max} the maximum measured ε_{NL} value.

An optimal σ value was obtained by using the Cross Verification method, with the following steps:

- 1) Assuming an initial value for σ starting from 0.01, with an increment of 0.01 up to 0.90.
- 2) Calculating the EEP values using Equation (7) for all assumed σ values from 0.01 to 0.90.
- 3) The optimal σ value was determined when EEP was at its minimum value.

Following the above procedures, the optimal σ value for the GRNN model was determined at 0.10, with the minimum EEP value of 3.45%. Consequently, the GRNN model developed would have a strong regression ability for prediction, without however the possibility of overfitting, for a greater general application ability.

3.3.2 Testing of the GRNN model

After the training, the GRNN model was tested using the remaining 111 groups of field measured data, for verifying its learning ability and general application ability. To this end, the EEP method as expressed in Equation (7), relative error (RE) method, mean absolute error (MAE) method and Pearson correlation coefficient (r) method were used as the evaluation criteria [20] for the testing data groups.

RE , MAE and r were described as follows:

$$RE = \frac{\left| \hat{y}_i - y_i \right|}{y_i} \times 100\% \quad |_{i=1-111} \quad (8)$$

$$MAE = \frac{1}{111} \sum_{i=1}^{111} \left| \hat{y}_i - y_i \right| \quad (9)$$

In Equations (8) and (9), \hat{y}_i and y_i are defined in the same way as in Equation (7).

The Pearson correlation coefficient, r , is an indicator of the degree of correlation for the GRNN model developed. For the GRNN model structure for predicting ε_{NL} shown in Fig. 5, its Pearson correlation coefficient is expressed as follows:

$$r = \frac{\sum_{i=1}^{111} (\hat{y}_i - \bar{\hat{y}}) (y_i - \bar{y})}{\sqrt{\sum_{i=1}^{111} (\hat{y}_i - \bar{\hat{y}})^2 \sum_{i=1}^{111} (y_i - \bar{y})^2}} \quad (10)$$

Where, \hat{y}_i and y_i are defined in the same way as in Equation (7), $\bar{\hat{y}}$ and \bar{y} the mean value of \hat{y}_i and y_i , respectively.

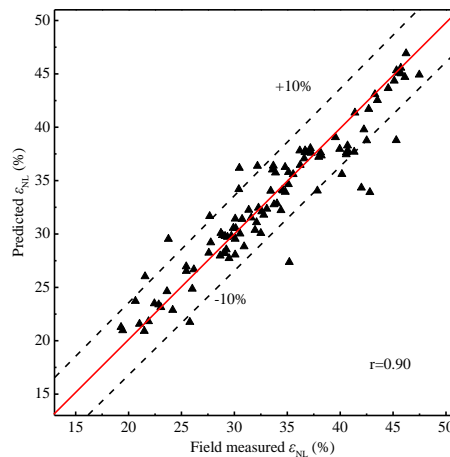


Fig. 6 Comparisons between the predicted and field measured ε_{NL} using the GRNN model based on the testing data of the 111 groups of field measured data

Using the above methods, the comparisons between the predicted and field measured ε_{NL} values based on the testing data of the 111 groups of field measured data are shown in Fig. 6. It can be seen that the correlation between the two was strong with an r value of 0.90, an EEP value of 6.45%. 95.4% of the predicted ε_{NL} values were within $\pm 10\%$ error band, with an MAE of 2.02%. These results suggested that the developed GRNN model was able to predict the ε_{NL} with an acceptable accuracy.

4 A modeling study for the operating performances of an ASHP unit during frosting-defrosting using the GRNN model for predicting ε_{NL}

With the availability of the GRNN model for predicting ε_{NL} , a modeling study was carried out to investigate the operating performances of an ASHP unit in terms of ε_{NL} at different T_a , RH and t_f . The study results are presented in this Section.

4.1 Predicted ε_{NL} values of an ASHP unit at different defrosting initiating time

At a constant ambient air condition, the influences of different defrost initiating time on ε_{NL} are shown in Fig. 7. It can be seen that at a constant ambient air temperature of -3°C and relative humidity of 70%, the predicted ε_{NL} was firstly decreased with a longer frosting period or defrosting initiating time. The ε_{NL} reached its minimum value of 31.9%. Afterwards, ε_{NL} was actually increased with an increase in t_f .

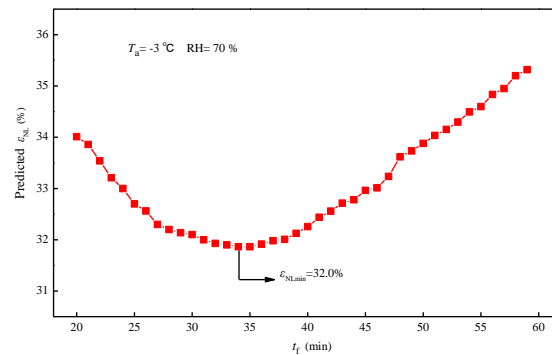


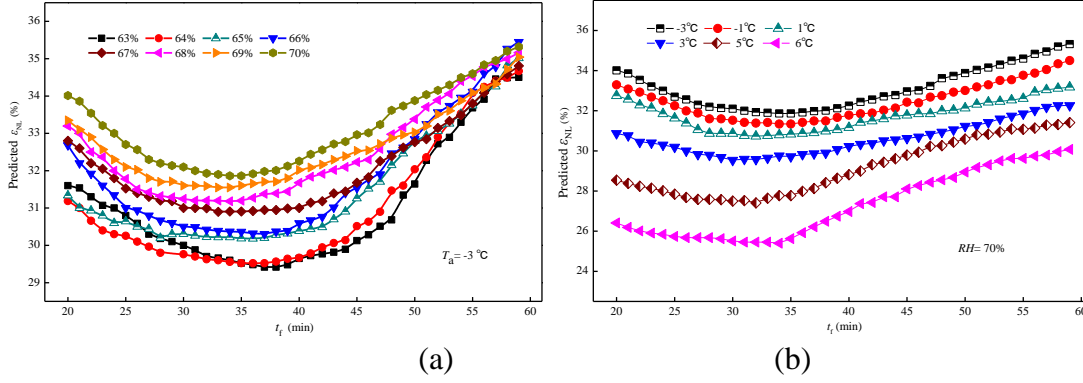
Fig. 7 Predicted ε_{NL} of an ASHP unit at different defrosting initiating time using the GRNN model

The modeling study results clearly demonstrated that at a fixed operating ambient condition, different defrosting initiating time, as a result of using different defrosting initiating strategies, would impact the operating performances of an ASHP in terms of ε_{NL} . As seen, there may exist an optimal defrosting initiating time at which ε_{NL} would be at its minimum.

4.2 Predicted ε_{NL} values of an ASHP unit at different ambient air conditions

The predicted influences of ambient air temperature and relative humidity on ε_{NL} using the GRNN model are illustrated in Fig. 8. From Fig. 8(a), it can be seen that at a fixed ambient air temperature of -3°C , the predicted ε_{NL} values were increased with an increase in relative humidity, due to a higher faster frosting rate at a higher relative humidity. On the other hand, at each of the fixed ambient relative humidity, similar variation trend of decreasing-increasing in ε_{NL} to that shown in Fig. 7 also demonstrated.

Furthermore, as seen from Fig. 8(b), at a fixed relative humidity, the predicted ε_{NL} values were increased with a decrease in ambient air temperature, mainly due to a lower ambient air temperature. In addition, at each fixed ambient air temperature, similar variation of decreasing-increasing in ε_{NL} to that shown in Fig. 7 was also demonstrated.



(a) Predicted ε_{NL} of an ASHP unit at varying relative humidity but a constant ambient air temperature

(b) Predicted ε_{NL} of an ASHP unit at varying ambient air temperature but a constant relative humidity

Fig. 8 Predicted ε_{NL} of an ASHP unit at different ambient air conditions

5. Conclusions

In this paper, a new performance index for ASHPs with frosting and defrosting operations based on the nominal output capacity has been proposed and a related modeling study carried out. The following conclusions may be drawn:

(1) To comprehensively and conveniently evaluate the actual operating performances of an ASHP unit with frosting and defrosting operations, the loss coefficient in the nominal output heating energy was proposed as the new performance index. The proposed loss coefficient was actually based on the nominal output heating capacity of an ASHP unit, which was readily available for the ASHP unit’s manufacturers and stayed unchanged irrespective when and where the ASHP unit was used. This would therefore provide a comprehensive and convenient way for evaluating the actual operating performances of ASHPs with frosting-defrosting operation and a guideline to system designer for properly sizing ASHP units.

(2) A detailed analysis of the 473 groups of field measured data for a field ASHP suggested the proposed new index of loss coefficient in the nominal output heating energy, ε_{NL} , was influenced by the ambient air temperature, relative humidity and the defrosting initiating time.

(3) A 4-layer GRNN model for predicting the ε_{NL} of the field ASHP unit was subsequently developed, using ambient air temperature, relative humidity and defrosting initiating time as input and ε_{NL} as the only output. 76.5% of the totally 473 groups of field measured data were used for training the GRNN model and the remaining 23.5% for testing the GRNN model established. The testing results demonstrated that the GRNN model for predicting ε_{NL} was of an acceptable accuracy.

(4) A modeling study using the GRNN model was carried out to exam how varying ambient air conditions and defrosting initiating time may influence ε_{NL} . The study results showed that at a fixed ambient air temperature and relative humidity, increasing frosting duration or delaying defrosting initiating time would lead to a decreasing-increasing variation trend in ε_{NL} , suggesting there may exist an optimal defrosting initiating time at which ε_{NL} would be at its minimum. On the other hand, at a fixed ambient air temperature, ε_{NL} would be increased with an increase in ambient air relative humidity, due to a faster frosting rate at higher relative

humidity. Furthermore, at a fixed relative humidity, ε_{NL} would be increased with a decrease in ambient air temperature, as a result of a lower ambient air temperature.

Acknowledgements

This work was supported partially by the National Natural Science Foundation of China (Grant No. 51178015), National Twelfth Five-year Science & Technology Support Plan (Grant No. 2011BAJ03B10), Training Plan of Top-notch Talent Youth, and the New-Star of Science and Technology supported by Beijing City.

References

- 1 Qu ML, Xia L, Deng SM, Jiang YQ. A study of the reverse cycle defrosting performance on a multi-circuit outdoor coil unit in an air source heat pump – Part I: Experiments. *Applied Energy*, 91(1): 274-280, 2012.
- 2 Wang RZ, Zhang C, Zhai XQ. Discussion on the design elements of air source heat pump air-conditioning, heating and hot water system for residential uses. *Chinese Journal of Refrigeration Technology*, (1): 32-41, 2014. [In Chinese]
- 3 Ma YT, Dai BM. Analysis of air-source heat pump for room heating. *Refrigeration and Air-conditioning*, 13(7): 6-11, 2013. [In Chinese]
- 4 Yue H, Li HY, Jiang Y. Realization of substituting coal with electricity and enhancing the efficiency of electricity allocation by using air source heat pump. *Energy of China*, 38(11): 7-13, 2016. [In Chinese]
- 5 Li CL. Hotspot Analysis of air source heat pump. *Chinese Journal of Refrigeration Technology*, 38(S1): 78-84, 2018. [In Chinese]
- 6 Wang W, Liu JD, Sun YY, Wu X, Bai XX, Zhu JH. Key problems and countermeasures for air-source heat pump under whole working conditions in Beijing. *Journal of HV & AC*, 47(1): 20-27, 2017. [In Chinese]
- 7 Bai XX, Sun YY, Wang W, Liu JD, Wu X. Field research on operating performance of air source heat pump under low temperature conditions in Beijing. *Building Science*, 33(10): 53-59, 2017. [In Chinese]
- 8 Dong JK, Deng SM, Jiang YQ, Xia L, Yao Y. An experimental study on defrosting heat supplies and energy consumptions during a reverse cycle defrost operation for an air source heat pump. *Applied Thermal Engineering*, 37(5): 380-387, 2012.
- 9 Wang W, Xiao J, Guo QC, Lu WP, Feng YC. Field test investigation of the characteristics for the air source heat pump under two typical mal-defrost phenomena. *Applied Energy*, 88(12): 4470-4480, 2011.
- 10 Song MJ, Deng SM, Pan DM, Mao N. An experimental study on the effects of downwards flowing of melted frost over a vertical multi-circuit outdoor coil in an air source heat pump on defrosting performance during reverse cycle defrosting. *Applied Thermal Engineering*, 67(1-2): 258-265, 2014.
- 11 ASHRAE Handbook: heating, ventilating, and air-conditioning systems and equipment. ASHRAE Inc, 2012
- 12 Jan K, Peter C, Ari R. Heating and Cooling of Buildings Design for Efficiency. CRC Press, 447-452, 2010.
- 13 Zhu JH, Sun YY, Wang W, Deng SM, Ge YJ, Li LT. Developing a new frosting map to guide defrosting control for air-source heat pump units. *Applied Thermal Engineering*, 90: 782-791, 2015.
- 14 Lu YQ. Design handbook for heating and air conditioning. Beijing: China Architecture & Building Press, 2008. [In Chinese]
- 15 Shi WX, Wang BL, Shao SQ. Design of small capacity air conditioners and heat pumps. Beijing: China Architecture & Building Press, 2013. [In Chinese]

- 16 AMEEN FR. Study of frosting of heat pump evaporators. *ASHRAE Trans*, 99: 61-71, 1993.
- 17 Jiang YQ, Yao Y, Ma ZL. Calculation of the loss coefficient for frosting-defrosting of air source heat pumps. *Journal of HV & AC*, 30(5): 24-26, 2004. [In Chinese]
- 18 Zhu JH, Sun YY, Wang W, Ge YJ, Li LT, Liu JD, Zhong AX. Field test investigation on the mal-defrosting of air source heat pump under the typical condition of hot summer and cold winter region. *Building Science*, 30(12): 15-19, 2014. [In Chinese]
- 19 Li N, Shi WX, Wang BL, Li XT. Performance model of general air source heat pump in a single frost /defrost cycle. *Journal of Refrigeration*, 36(2): 1-7, 2015.
- 20 SPECHT DF. A general regression neural network. *IEEE Transactions on Neural Networks*, 2(6): 568-576, 1991.
- 21 Li Q, Meng QL, Cai JJ, Yoshino H, Mochida A. Predicting hourly cooling load in the building: A comparison of support vector machine and different artificial neural networks. *Energy Conversion and Management*, 50(1): 90-96, 2009.
- 22 Yu JM, Li M, Shu F. Application of GRNN-algorithm on load modeling of power system. *Proceedings of the CSU-EPSA*, 21(1): 104-107, 2009.
- 23 Ge YJ, Sun YY, Wang W, Zhu JH, Li LT, Liu JD. Field test study of a novel defrosting control method for air-source heat pumps by applying tube encircled photoelectric sensors. *International Journal of Refrigeration*, 66: 133-144, 2016.
- 24 Zhu JH, Sun YY, Wang W, Ge YJ, Li LT, Liu JD. A novel Temperature–Humidity–Time defrosting control method based on a frosting map for air-source heat pumps. *International Journal of Refrigeration*, 54: 45-54, 2015.
- 25 Akoglu H. User's guide to correlation coefficients. *Turkish Journal of Emergency Medicine*, 18: 91-93, 2018.
- 26 Li N, Xia L, Deng SM, Xu XG, Chan MY. Dynamic modeling and control of a direct expansion air conditioning system using artificial neural network. *Applied Energy*, 91(1): 290-300, 2012.
- 27 Diaz G, Sen M, Yang KT, McClain RL. Simulation of heat exchanger performance by artificial neural networks. *Int J HVAC Res*, 5(3): 195–208, 1999.
- 28 Anderson CW, Hittle DC, Katz AD, Kretchmar RM. Synthesis of reinforcement learning, neural networks and PI control applied to a simulated heating coil. *Artificial Intelligence Eng*, 11(4): 421–9, 1997.
- 29 Borra S, Ciaccio AD. Measuring the prediction error: A comparison of cross-validation, bootstrap and covariance penalty methods. *Computational Statistics & Data Analysis*, 54(12): 2976-2989, 2010.



Asian Heat Pump Thermal Storage Technologies Network

To promote energy savings and combat global warming, there is an urgent need to spread efficient heat pump and thermal storage technologies on the demand side. Countries in Asia, which are enjoying rapid economic growth, should coordinate with one another to spread this technology. Five to ten years from now, Asia will become a global economic powerhouse and heat pump technologies will play a considerable role in all sectors. Asian countries will therefore need to address common issues and problems that have already been faced in Europe and North America. Concerning the building of connections and networks among countries, it is essential to share information on diffusion policies, technology trends, applications, etc., and then to make incremental improvements. Further, situations which can or should be handled through collaboration should be handled flexibly, on a case-by-case basis, with the collaboration of all countries. In order to encourage the use and development of heat pump and thermal storage technologies in Asian countries we have established AHPNW in 2011.

Participating Countries and Entities

CHINA: China Academy of Building Research (CABR)

INDIA: Indian Society of Heating, Refrigerating and Air Conditioning Engineers (ISHRAE)

JAPAN: Heat Pump and Thermal Storage Technology Center of Japan (HPTCJ)

KOREA: Korea Testing Laboratory (KTL)

VIETAM: Hanoi University of Science and Technology (HUST)

THAILAND: King Mongkut's University of Technology Thonburi (KMUTT)

INDONESIA: Heating, Cooling & Thermo Fluids Technology Indonesia (HCTFTI)

Please visit our website for more information.

⇒<http://www.hptcj.or.jp/e/ahpnw/tabid/571/language/en-US/Default.aspx>

